Scanning Tunneling Microscopy (STM) and Tunneling Spectroscopy (TS) of Heteropolyacid (HPA) Self-Assembled Monolayers (SAMS): Connecting Nano Properties to Bulk Properties

In Kyu Song[†] and Mark A. Barteau*

Department of Environmental & Applied Chemical Engineering,
Kangnung National University, Kangnung 210-702, Korea
*Center for Catalytic Science and Technology, Department of Chemical Engineering,
University of Delaware, Newark, Delaware 19716, U.S.A.
(*Received 19 February 2002 • accepted 3 April 2002*)

Abstract−Nanoscale investigation of Keggin-type heteropolyacid (HPA) self-assembled monolayers (SAMs) was performed by scanning tunneling microscopy (STM) and tunneling spectroscopy (TS) in order to relate surface properties of nanostructured HPA monolayers to bulk redox and acid properties of HPAs. Cation-exchanged, polyatom-substituted, and heteroatom-substituted HPAs were examined to see the effect of different substitutions. HPA samples were deposited on HOPG surfaces in order to obtain images and tunneling spectra by STM before and after pyridine adsorption. All HPA samples formed well-ordered monolayer arrays, and exhibited negative difference resistance (NDR) behavior in their tunneling spectra. NDR peaks measured for fresh HPA samples appeared at less negative potentials for higher reduction potentials of the HPAs. These changes could also be correlated with the electronegativities of the substituted atoms. Introduction of pyridine into the HPA arrays increased the lattice constants of the two-dimensional HPA arrays by ca. 6 Å. Exposure to pyridine also shifted NDR peak voltages of HPA samples to less negative values in the tunneling spectroscopy measurements. The NDR shifts of HPAs obtained before and after pyridine adsorption were correlated with the acid strengths of the HPAs. This work demonstrates that tunneling spectra measured by STM can fingerprint acid and redox properties of HPA monolayers on the nanometer scale.

Key words: Scanning Tunneling Microscopy (STM), Negative Differential Resistance (NDR), Heteropolyacids (HPAs), Self-assembled Monolayers, Redox and Acid Properties

INTRODUCTION

Scanning tunneling microscopy (STM) provides a way to observe individual molecules [Carroll et al., 2000] and even chemical reactions on single crystal surfaces [Chiang, 1997]. Examples of molecules imaged include carbon monoxide on Rh(111) [Cernota et al., 2000] and Ag(110) [Lee and Ho, 2000]; oxygen on Pd(111) [Steltenpohl and Memmel, 1999] and Pt(111) [Stipe et al., 1997]; benzoic acid on Cu(110) [Chen et al., 2000]; *m*-xylene and *p*-xylene on Rh(111) [Cernota et al., 1998]; and methoxy and formate species on Cu(110) [Silva et al., 1999]. An STM image contains both geometric and electronic information about the sample. Highly resolved STM images can distinguish between different molecules with very similar geometric structures and molecular sizes. For example, metal atoms on an alloy surface have been distinguished by their apparent height difference [Wouda et al., 1996], and metal phthalocyanines on Au(111) have been identified by metal d-orbital occupation-dependent images [Hipps et al., 1996]. Tunneling spectroscopy (TS), which probes only electronic states of surface species, has been utilized as a complementary technique to distinguish between chemically inequivalent sites or adsorbates with nearly iden-

tical geometric structures and sizes [Johansson et al., 1996]. The distinction is made based on differences in electronic structures. We have observed that individual molecules of soccer ball-like $H_3PW_{12}O_{40}$ and $H_3PMo_{12}O_{40}$ (whose molecular structures and dimensions are nearly identical) in a mixed array can be distinguished by their tunneling spectroscopy responses [Kaba et al., 2002]. In the case of organic molecules, tunneling spectroscopy measured for a single molecule on a metal surface has proven to be a valuable "fingerprint" method [Stipe et al., 1998].

Heteropolyacids (HPAs) are early transition metal oxygen anion clusters that exhibit a wide range of molecular sizes, compositions, and architectures [Pope and Müller, 1994]. Among various HPA structural classes, the Keggin-type [Keggin, 1933] HPAs have been widely employed as catalysts in homogeneous and heterogeneous systems for acid-base and oxidation reactions [Lee et al., 1995, 1997; Kozhevnikov, 1995; Hill and Prosser-McCartha, 1995; Choi et al., 2000; Park et al., 2000; Lee and Song, 2000]. One of the great advantages of HPA catalysts is that their catalytic properties can be tuned by changing the identity of charge-compensating countercations, heteroatoms, and framework metal atoms (polyatoms) [Song et al., 1991, 1997; Okuhara et al., 1996]. Recently, members of four HPA structural classes --Keggin-, Wells-Dawson-, Finke-Droege-, and Pope-Jeannin-Preyssler-type HPAs--have been successfully imaged in air using STM by depositing these molecules on graphite surfaces [Kaba et al., 1998]. Previous STM studies of HPAs showed that two-dimensional ordered arrays of these molecules on a graph-

---

ite surface exhibited a distinctive current-voltage (I-V) behavior referred to as negative differential resistance (NDR) in their tunneling spectra [Watson et al., 1992; Kaba et al., 1996, 1997, 1998, 2000; Song et al., 1996, 1998, 2002; Kinne and Barteau, 2000; Song and Barteau, 2002]. NDR behavior has been explained in terms of resonant tunneling through a double barrier quantum well [Maboudian et al., 1993], and has been observed consistently for the arrays of HPAs. We have shown that NDR peak voltages of HPAs are closely related to electronic properties and, in turn, to the redox potentials of HPAs [Kaba et al., 1996, 1997; Song et al., 1998, 2002; Kinne and Barteau, 2000]. NDR peak voltages can be influenced by the identity of the counter-cations, framework transition-metal atoms, heteroatoms, and adsorbed organic molecules.

In this work, nanoscale characterization of HPA monolayers was performed by scanning tunneling microscopy and tunneling spectroscopy in order to relate surface properties of nanostructured HPA monolayers to bulk redox and acid-base properties of HPAs. Keggin-type HPAs with different counter-cation, polyatom, and heteroatom substitutions were examined for this purpose. HPA samples were deposited on a highly oriented pyrolytic graphite (HOPG) surface in order to obtain images and tunneling spectra by STM before and after pyridine adsorption. The observed NDR peak voltages of HPA monolayers were correlated with the redox properties as well as with the acid properties of HPAs.

EXPERIMENTAL

1. Sample Preparation and Deposition

A series of the following HPAs were investigated to explore their redox properties: cation-exchanged $RPMo_{12}O_{40}$ ($R=H_3^+$, Cs_3^+, $Ba_{3/2}^{2+}$, $Zn_{3/2}^{2+}$, $Co_{3/2}^{2+}$, $Cu_{3/2}^{2+}$, Bi_1^{3+}), heteroatom-substituted and/or polyatom-substituted $H_nXW_{12}O_{40}$ ($X=P^{5+}$, Si^{4+}, B^{3+}, Co^{2+}) and $H_nXMo_{12}O_{40}$ ($X=P^{5+}$, Si^{4+}) HPAs. Commercially available $H_3PMo_{12}O_{40}$, $H_3PW_{12}O_{40}$, $H_4SiMo_{12}O_{40}$ and $H_4SiW_{12}O_{40}$ samples were obtained from Aldrich Chemical Co. $H_5BW_{12}O_{40}$ and $H_6CoW_{12}O_{40}$ samples were provided by Prof. Craig L. Hill at Emory University. Cation-exchanged HPAs were prepared by replacing all protons of $H_3PMo_{12}O_{40}$ with metal atoms, according to published methods [Ai, 1982]. Approximately 0.01 M aqueous solution of each HPA sample was prepared. A drop of solution was deposited on a freshly cleaved HOPG surface and allowed to dry in air for ca. 1 h at room temperature for STM imaging and TS measurements. Heteroatom-substituted $H_nXW_{12}O_{40}$ ($X=P^{5+}$, Si^{4+}, B^{3+}, Co^{2+}) HPAs were also examined to explore their acid properties. For this purpose, pyridine exposure was carried out by placing a drop of liquid pyridine on these previously deposited HPA samples and drying in air for ca. 1 h at room temperature. Reversibly adsorbed pyridine molecules were then removed by evacuating the sample at ca. 25 millitorr for 1 h at room temperature prior to the STM measurements.

2. STM Imaging and Tunneling Spectroscopy

STM images were obtained in air by using a Topometrix TMX 2010 instrument. Mechanically formed Pt/Ir (90/10) tips were used as probes. Scanning was done in the constant current mode at a positive sample bias of 100 mV and tunneling current of 1-2 nA. All STM images presented in this work are unfiltered, and the reported periodicities (lattice constants) represent average values determined by performing two-dimensional Fast Fourier Transformation (2D-

FFT) analyses on at least three images for each sample which were obtained by using different tips. Tunneling spectra were measured in air. Both Topometrix TMX 2010 and LK Technologies LK-1000 STM instruments were used to confirm consistency and reproducibility of tunneling spectra. To measure a tunneling spectrum, the sample bias was ramped from −2 to +2 V with respect to the tip and the tunneling current was monitored. The voltage axis in the tunneling spectrum represents the potential applied to the sample relative to that of the tip. TS measurements were performed at least ten times each by using at least three different tips for each sample to obtain more accurate and reproducible results, and to provide a basis for statistical analyses.

RESULTS AND DISCUSSION

1. Self-assembled HPA Arrays

Fig. 1(a) shows the molecular structure of the pseudo-spherical (T_d symmetry) Keggin-type $[PMo_{12}O_{40}]^{3-}$ heteropolyanion constructed from X-ray crystallography data [Strandberg, 1975]. The molecular structure of $[PMo_{12}O_{40}]^{3-}$ consists of a heteroatom, P, at the center of the anion cluster, tetrahedrally coordinated to four oxygen atoms. This tetrahedron is surrounded by twelve MoO_6 octahedra. The van der Waals diameter along the 3-fold axis of symmetry is 11.97 Å. Fig. 1(b) shows the three-dimensional array of HPAs comprising heteropolyanions, protons, cations, water, and/or organic molecules, called the secondary structure [Misono, 1987]. The counter-cations are located in the interstitial spaces between heteropolyanions. The primary structure, the Keggin structure [Keggin, 1933], of the heteropolyanion is relatively stable. However, the secondary structure is very labile and may change in different environments by either increasing or decreasing the interstitial space between heteropolyanions [Misono, 1987]. Fig. 1(c) and Fig. 1(d) show the STM image and
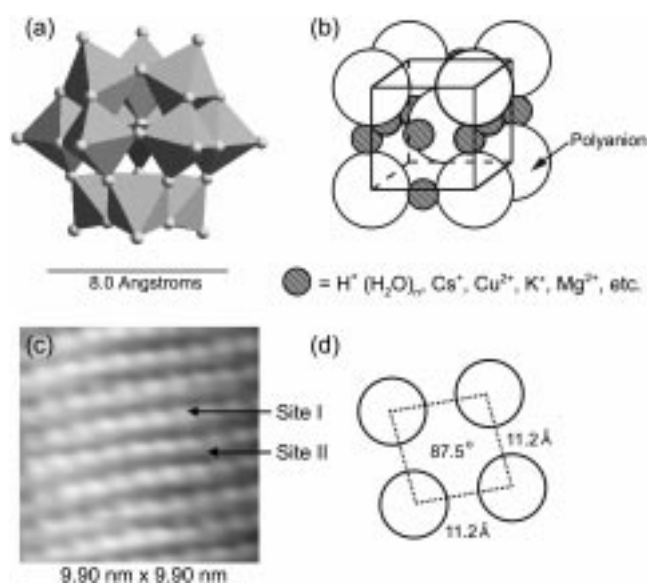

Fig. 1. (a) Polyhedral representation of the molecular structure of the pseudo-spherical Keggin-type $[PMo_{12}O_{40}]^{3-}$ heteropolyanion (primary structure), (b) schematic of the secondary structure of heteropolyacids, (c) STM image of $H_4SiW_{12}O_{40}$ array on graphite, and (d) unit cell of $H_4SiW_{12}O_{40}$ array on graphite.

unit cell of a $H_4SiW_{12}O_{40}$ array on graphite, respectively. The structure of the $[SiW_{12}O_{40}]^{4-}$ anion is the same as that of the $[PMo_{12}O_{40}]^{3-}$ anion in Fig. 1(a). The STM image clearly shows the formation of a self-assembled and well-ordered array on the graphite surface. The periodicity and included angle of the unit cell constructed on the basis of lattice constants determined from 2D-FFT are 11.2 Å and 87.5°, respectively. The measured periodicity is in good agreement with lattice constants of the Keggin-type HPAs obtained by STM [Kaba et al., 1996, 1997, 1998, 2000; Song et al., 1998; Kinne and Barteau, 2000] and X-ray crystallography [Strandberg, 1975; Brown et al., 1977]. All HPA samples examined in this work formed well-ordered arrays on graphite surfaces over scan areas of at least 200 Å by 200 Å.

2. NDR Measurements on HPA Monolayers

Fig. 2(a) shows the typical tunneling spectrum taken atop sites (Site I) in the image of the $H_4SiW_{12}O_{40}$ array in Fig. 1(c). The spectrum taken at Site I exhibits distinctive I-V behavior known as negative differential resistance (NDR), showing an NDR peak at −1.20 V. The NDR peak voltage is taken as the voltage at which the maximum current is observed in this region. A tunneling spectrum taken
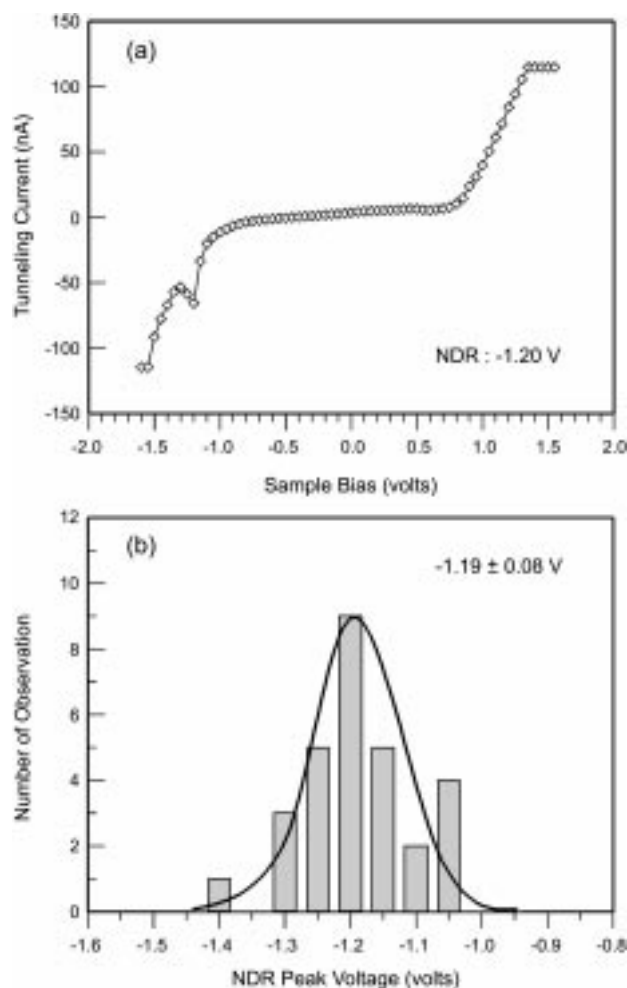
at the interstitial space (Site II) showed the same I-V response as bare graphite, indicating that the two-dimensional array of $H_4SiW_{12}O_{40}$ on graphite is a monolayer, as previously demonstrated for other HPAs [Kaba et al., 1996, 1997, 1998, 2000; Song et al., 1998; Kinne and Barteau, 2000]. The tunneling spectroscopy measurements atop the bright corrugations (Site I) were carried out several times with at least three different tips to obtain more accurate and reproducible results, and to provide a basis for statistical analyses. Fig. 2(b) shows the distribution of NDR peak voltages of the $H_4SiW_{12}O_{40}$ sample. The statistical average of NDR peak voltage of the $H_4SiW_{12}O_{40}$ array was found to be −1.19±0.08 V. NDR peak voltages of each HPA sample reported below were determined in the same way.

3. Probing Redox Properties of HPAs

The STM images in this work were obtained at positive sample biases with respect to the tip, i.e., electrons flow from tip to sample in the normal mode of operation. NDR behavior in the tunneling spectra of HPAs is observed at negative sample biases, i.e., when electrons tunnel from sample to tip. It has been demonstrated that the NDR behavior of nanostructured HPA arrays measured by STM is closely related to the electronic properties of these materials, and may serve as a diagnostic of their redox properties [Kaba et al., 1996, 1997; Song et al., 1998; Kinne and Barteau, 2000]. A previous result [Kaba et al., 1996] has shown that the NDR peaks appeared at less negative applied voltages when the protons of the $H_3PMo_{12}O_{40}$ were replaced by more electronegative cations such as Cu^{2+}; the NDR peaks shifted to higher negative voltages when the protons were replaced by less electronegative cations such as Cs^+. By plotting the reduction potentials [Ai, 1982] of cation-exchanged HPAs against the electronegativities of the counter-cations defined by Tanaka [Tanaka and Ozami, 1967], it was shown that as more electronegative cations were substituted for less electronegative ones, the reduction potential increased, and vice versa. More comprehensive trends of reduction potential of cation-exchanged HPAs and electronegativity of counter-cations with respect to NDR peak voltages of the HPAs were well established by investigating a set of cation-exchanged $RPMo_{12}O_{40}$ (R=H_3^+, Cs_3^+, $Ba_{3/2}^{2+}$, $Zn_{3/2}^{2+}$, $Co_{3/2}^{2+}$, $Cu_{3/2}^{2+}$, Bi_1^{3+}) HPAs. These cations cover a wide range of Tanaka electrone-
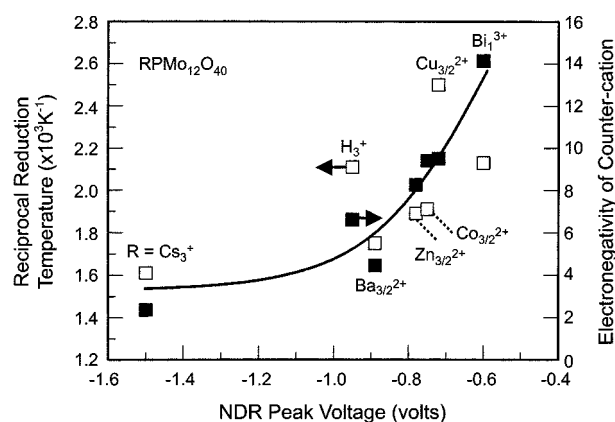

Fig. 2. (a) I-V spectrum taken at Site I in the STM image of $H_4SiW_{12}O_{40}$ in Fig. 1(c), and (b) frequency of NDR peak voltages of $H_4SiW_{12}O_{40}$ monolayer arrays exhibiting monomodal distribution with a statistical average of −1.19± 0.08 V.

Fig. 3. Correlation between NDR peak voltage of cation-exchanged $RPMo_{12}O_{40}$ (R=H_3^+, Cs_3^+, $Ba_{3/2}^{2+}$, $Zn_{3/2}^{2+}$, $Co_{3/2}^{2+}$, $Cu_{3/2}^{2+}$, Bi_1^{3+}) HPAs and Tanaka electronegativity of the counter-cation (filled squares), and between NDR peak voltage and reciprocal reduction temperature of the HPAs (open squares).
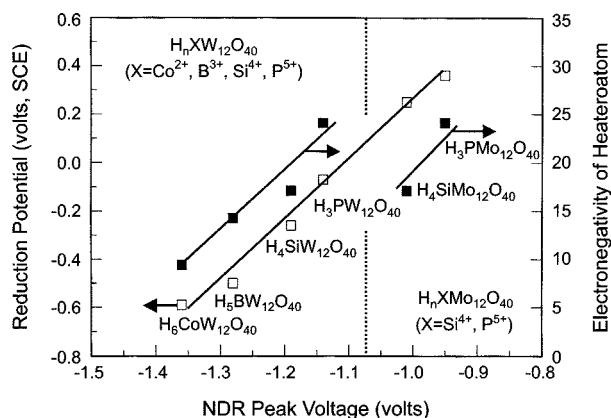
Fig. 4. Correlation between NDR peak voltage and reduction potential of HPAs with different heteroatom and/or polyatom substitutions, established for families of $H_nXW_{12}O_{40}$ ($X=P^{5+}$, Si^{4+}, B^{3+}, Co^{2+}) and $H_nXMo_{12}O_{40}$ ($X=P^{5+}$, Si^{4+}) HPAs.

gativities [Tanaka and Ozami, 1967]. Fig. 3 includes the reciprocal reduction temperatures of cation-exchanged HPAs taken from the literature [Ai, 1982] and the Tanaka electronegativities of the counter-cations, plotted with respect to the NDR peak voltages of cation-exchanged HPAs. The NDR peak voltages appeared at less negative values with increasing reduction potential of the HPAs and with increasing electronegativity of the counter-cation. HPA salts with more electronegative counter-cations were characterized by higher reduction potentials and showed NDR at less negative applied voltages. The Tanaka electronegativity scale takes into account the electron-donating and -accepting ability of the atom. A possible explanation for these results is that more electronegative cations facilitate electron transfer to the heteropolyanion in reducing environments, by providing a route for electron delocalization [Kim et al., 1991].

Fig. 4 shows the relationship between NDR peak voltage of heteroatom-substituted $H_nXW_{12}O_{40}$ ($X=P^{5+}$, Si^{4+}, B^{3+}, Co^{2+}) and $H_nXMo_{12}O_{40}$ ($X=P^{5+}$, Si^{4+}) HPAs and Tanaka electronegativity of the heteroatom, and between NDR voltage and reduction potential of the HPA samples. Reduction potentials of $H_nXW_{12}O_{40}$ ($X=P^{5+}$, Si^{4+}, B^{3+}, Co^{2+}) and $H_nXMo_{12}O_{40}$ ($X=P^{5+}$, Si^{4+}) HPAs were taken from the literature [Alternau et al., 1975; Okuhara et al., 1996; Sadakane and Steckhan, 1998]. As the electronegativity of the heteroatom increased, NDR peak voltages observed for each HPA family appeared at less negative values, and the reduction potential increased. This result supports our conclusion that more reducible HPAs show NDR behavior at less negative applied voltages in their tunneling spectra. This conclusion appears to hold across different families of heteroatom-substituted HPAs. The NDR peak voltage and reduction potential dependences on heteroatom electronegativity show the same trends as for cation-exchanged HPAs (Fig. 3). A quantum chemical molecular orbital study accompanied by experiments for heteroatom-substituted $H_nXMo_{12}O_{40}$ ($X=As^{5+}$, P^{5+}, Ge^{4+}, Si^{4+}) HPAs [Eguchi et al., 1988] revealed that reduction potentials of the HPAs increased in the following order; $Si^{4+}<Ge^{4+}<P^{5+}<As^{5+}$. Simple calculation of the Tanaka electronegativity of the heteroatom in these HPAs yields the following sequence: Si^{4+} (17.1)$<Ge^{4+}$ (18.1)$<As^{5+}$ (24.0)$\approx P^{5+}$ (24.1). These trends are consistent with the results shown in Fig. 4.

Fig. 4 also shows the effect of polyatom substitution on the reduction potential and NDR peak voltage of HPAs. A set of data points $H_4SiW_{12}O_{40}$-$H_4SiMo_{12}O_{40}$ and $H_3PW_{12}O_{40}$-$H_3PMo_{12}O_{40}$ show that NDR peak voltages of polyatom-substituted HPAs appeared at less negative values with increasing reduction potential of the HPAs, as observed for cation-exchanged and heteroatom-substituted HPAs. Considering that molybdenum is less electronegative than tungsten, these data also reveal that NDR peak voltages of polyatom-substituted HPAs appeared at less negative values and reduction potential of the HPAs increases with decreasing electronegativity of the polyatom. Surprisingly, the trends of polyatom electronegativity with respect to NDR peak voltage and reduction potential of polyatom-substituted HPAs are the opposite of those seen for the cation-exchanged HPAs and for heteroatom-substituted HPAs. These results were also confirmed by a previous STM study [Song and Barteau, 2002] investigating polyatom-substituted $H_nPW_{11}MO_{40}$ ($M=W^{6+}$, Mo^{6+}, V^{5+}) HPAs. Within this HPA family, it was also observed that the NDR peak voltages of $H_nPW_{11}MO_{40}$ ($M=W^{6+}$, Mo^{6+}, V^{5+}) arrays appeared at less negative values with increasing reduction potential of the HPAs, and with decreasing electronegativity of the substituted polyatom. In fact, the effect of polyatom substitution on the NDR peak voltage and reduction potential of HPAs is somewhat complicated. In the case of $H_{3+x}PMo_{12-x}V_xO_{40}$ (x=0-3) HPAs, NDR peak voltages of these HPAs did not vary monotonically with the number of vanadium ions substituted (note that vanadium is less electronegative than molybdenum). Instead, the NDR peak appeared at the least negative voltage when x=2. Nonetheless, NDR peak voltages were well correlated with reduction potentials across the composition range above. In a series of polyatom-substituted $H_3PMo_{12-x}W_xO_{40}$ (x=0-12) HPAs [Song et al., 1998], however, it was observed that NDR peak voltages of these HPAs shifted to less negative values and their reduction potentials increased in a monotonic fashion with increasing Mo content. When considering that molybdenum is less electronegative than tungsten, the dependence of NDR peak voltage on the polyatom electronegativity observed for $H_3PMo_{12-x}W_xO_{40}$ (x=0-12) HPAs shows the same trend as that shown in Fig. 4.

A molecular orbital study [Weber, 1994] for $H_nPM_{12-x}V_xO_{40}$ ($M=Mo^{6+}$, W^{6+}; x=0-3) HPAs revealed that the energy gap between the HOMO (highest occupied molecular orbital) and the LUMO (lowest unoccupied molecular orbital) was consistent with reduction potentials of the HPAs; the more reducible HPAs showed the smaller energy gaps. It also showed that the HOMO for all HPAs consists primarily of nonbonding p-orbitals on the oxygens of the HPAs, while the LUMO consists of an antibonding combination of d-orbitals on the metal centers and p-orbitals on the neighboring bridging oxygens. Thus, substitution of V ions into either the Mo or W framework did not affect the energies of the HOMOs since they are almost entirely centered on the oxygens. However, the same substitution stabilized the LUMOs because these orbitals derive in part from V d-orbitals which have been assumed to be more stable than those of Mo and W. This suggests that electrons added to the V-substituted HPAs should be localized on the vanadium centers. Therefore, it is inferred that electrons added to the polyatom-substituted HPAs are localized on the less electronegative metal center. The less electronegative polyatom in the HPAs is much more efficient in the role of electron localization.
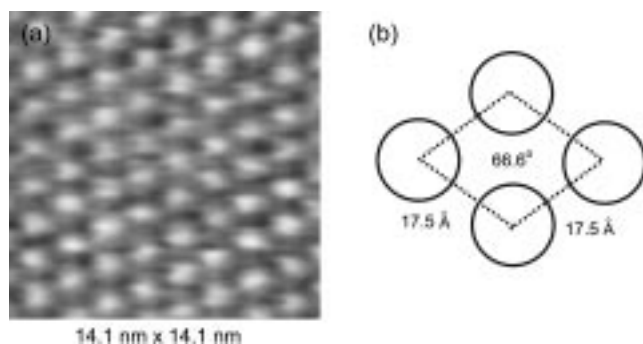
Fig. 5. (a) STM image of pyridine-exposed $H_4SiW_{12}O_{40}$ array on graphite, and (b) unit cell of pyridine-exposed $H_4SiW_{12}O_{40}$ array on graphite.

4. Probing Acid Properties of HPAs

In the 3-dimensional structure of the pyridinium salt of $[PW_{12}O_{40}]^{3-}$, it was reported that the pyridine molecules were paired around H^+, forming (C_5H_5N)-H^+-(NC_5H_5) cations [Hashimoto and Misono, 1994]. The interaction of pyridine with HPA monolayers was imaged by STM. Fig. 5 shows the STM image and unit cell of a $H_4SiW_{12}O_{40}$ array obtained after pyridine exposure. The STM image clearly shows the formation of self-assembled and well-ordered HPA arrays on the graphite surface after pyridine exposure. As already shown in Fig. 1(c) and Fig. 1(d), the periodicity and included angle of the unit cell observed for fresh $H_4SiW_{12}O_{40}$ HPA were 11.2 Å and 87.5°, respectively. Unlike the fresh HPA sample array, the pyridine-exposed $H_4SiW_{12}O_{40}$ HPA sample formed a roughly hexagonal array (included angle=66.6°) with periodicity of 17.5 Å. Compared to that of fresh sample, the periodicity of the pyridine-exposed $H_4SiW_{12}O_{40}$ array increased by ~6 Å, roughly the molecular size of pyridine. This result demonstrates that pyridine molecules are bound at the acid sites in the interstitial space between heteropolyanions in the two-dimensional surface arrays, serving as spacer molecules, in a similar manner to the bonding in 3-dimensional solids. These results also indicate that two-dimensional HPA arrays were rearranged and expanded upon pyridine exposure. However, the pyridinium ions, like other charge compensating cations in these arrays [Song et al., 1996], were not imaged directly.

The interaction of pyridine with HPA monolayers was also probed by tunneling spectroscopy measurements. Tunneling spectroscopy showed that the average value of NDR peak voltages observed for fresh $H_4SiW_{12}O_{40}$ sample was -1.19 ± 0.08 V (Fig. 2), while that for the pyridine-exposed $H_4SiW_{12}O_{40}$ sample was found -0.85 ± 0.07 V. Introduction of electron-rich pyridine molecules into $H_4SiW_{12}O_{40}$ arrays leads to an NDR voltage shift of 0.34 V, from -1.19 V to -0.85 V. The shift of NDR peak voltages of HPA samples to less negative applied voltages after pyridine adsorption reflects the replacement of protons with pyridinium ions. This effect on NDR position is similar to that obtained by exchanging more electronegative counter cations for protons. It can be inferred that the strong interaction of base molecules with acid sites of HPA arrays may give rise to large NDR shifts. The magnitudes of the NDR peak shifts of different HPAs measured before and after pyridine adsorption may serve as a fingerprint of their acid properties. Fig. 6 shows the correlation between NDR voltage shifts for as-deposited versus pyridine-exposed HPA arrays, and the acid strengths of $H_nXW_{12}O_{40}$ (X
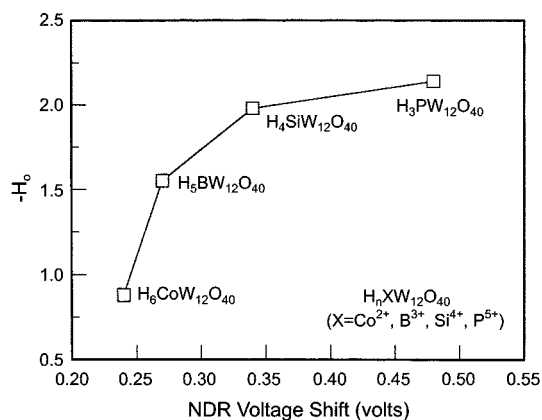
Fig. 6. Correlation between acid strengths of $H_nXW_{12}O_{40}$ (X=P^{5+}, Si^{4+}, B^{3+}, Co^{2+}) HPAs and their NDR voltage changes after pyridine exposure.

=P^{5+}, Si^{4+}, B^{3+}, Co^{2+}) samples reported in the literature [Okuhara et al., 1994]. The acid strength of $H_nXW_{12}O_{40}$ (X=P^{5+}, Si^{4+}, B^{3+}, Co^{2+}) samples track the NDR peak voltage shifts upon pyridine exposure. $H_3PW_{12}O_{40}$ has the highest acid strength among the samples examined and exhibits the largest NDR peak shift upon pyridine exposure. This suggests that the change in the electronic environment of the heteropolyanion upon proton transfer is greatest for the strongest proton donor. Thus, we conclude that NDR voltage shifts of HPAs measured by STM can be used to track their acid properties.

CONCLUSIONS

STM studies of nanostructured HPA monolayers were successful in relating surface properties to bulk redox and acid properties of HPAs. All Keggin samples formed well-ordered monolayer arrays, and exhibited negative difference resistance (NDR) behavior in their tunneling spectra. NDR peak voltages for both cation-exchanged and heteroatom-substituted HPAs appeared at less negative values with increasing reduction potential of the HPAs and with increases in the electronegativity of counter-cations or of the central heteroatom. NDR peak voltages of polyatom-substituted HPAs also appeared at less negative values with increasing reduction potential of the HPAs, but with decreasing electronegativity of the polyatom. All our results consistently support the conclusion that more reducible HPAs show NDR behavior at less negative applied voltages. Introduction of pyridinium cations into the HPA arrays increased their periodicity and shifted their NDR peak voltages to less negative values. The NDR shift of HPAs obtained before and after pyridine adsorption was correlated with the acid strengths of HPA samples. The NDR shift may serve as a diagnostic for the acid properties of HPAs. Thus STM and tunneling spectroscopy permit one to determine the chemical properties of self-assembled HPA monolayers on the molecular scale.

ACKNOWLEDGEMENTS

fund from KOSEF (R01-2001-00411).

REFERENCES

Ai, M., "Effects of Cations Introduced into 12-Molybdophosphoric Acid on the Catalyst Properties," *Appl. Catal.*, **4**, 245 (1982).

Altenau, J. J., Pope, M. T., Prados, R. A. and So, H., "Models for Heteropoly Blues. Degree of Valence Trapping in Vanadium(IV)- and Molybdenum(V)-substituted Keggin Anions," *Inorg. Chem.*, **14**, 417 (1975).

Brown, G. M., Noe-Spirlet, M. R., Busing, W. R. and Levy, H. A., "Dodecatungstophosphoric Acid Hexahydrate, $(H_5O_2^+)_3(PW_{12}O_{40}^{3-})$. The True Structure of Keggin's Pentahydrate from Single-crystal X-ray and Neutron Diffraction Data," *Acta. Cryst. B*, **33**, 1038 (1977).

Carroll, D. L., Czerw, R., Tekeleab, D. and Smith, Jr., D. W., "Anomalous Periodic Structure of Polypropylene Chains Observed with Scanning Tunneling Microscopy," *Langmuir*, **16**, 3574 (2000).

Cernota, P., Yoon, H. A., Salmeron, M. and Somorjai, G. A., "The Structure of para-Xylene and meta-Xylene Adsorbed on Rh(111) Studied by Scanning Tunneling Microscopy," *Surf. Sci.*, **415**, 351 (1998).

Cernota, P., Rider, K., Yoon, H. A., Salmeron, M. and Somorjai, G. A., "Dense Structures Formed by CO on Rh(111) Studied by Scanning Tunneling Microscopy," *Surf. Sci.*, **445**, 249 (2000).

Chen, Q., Perry, C. C., Frederick, B. G., Murray, P. W., Haq, S. and Richardson, N. V., "Structural Aspects of the Low-temperature Deprotonation of Benzoic Acid on Cu(110) Surfaces," *Surf. Sci.*, **446**, 63 (2000).

Chiang, S., "Scanning Tunneling Microscopy Imaging of Small Adsorbed Molecules on Metal Surfaces in an Ultrahigh Vacuum Environment," *Chem. Rev.*, **97**, 1083 (1997).

Choi, J. S., Song, I. K. and Lee, W. Y., "A Composite Catalytic Membrane Reactor Using Heteropolyacid-blended Polymer Membrane," *Korean J. Chem. Eng.*, **17**, 280 (2000).

Eguchi, K., Seiyama, T., Yamazoe, N., Katsuki, S. and Taketa, H., "Electronic Structures of $XMo_{12}O_{40}$ Heteropolyanions (X=P, As, Si, and Ge) and Their Reduction Behavior," *J. Catal.*, **111**, 336 (1988).

Hashimoto, M. and Misono, M., "$[(C_5H_5N)_2H]_3[PW_{12}O_{40}]$," *Acta Cryst. C*, **50**, 231 (1994).

Hill, C. L. and Prosser-McCartha, C. M., "Homogeneous Catalysis by Transition Metal Oxygen Anion Clusters," *Coord. Chem. Rev.*, **143**, 407 (1995).

Hipps, K. W., Lu, X., Wang, X. D. and Mazur, U., "Metal d-Orbital Occupation-Dependent Images in the Scanning Tunneling Microscopy of Metal Phthalocyanines," *J. Phys. Chem.*, **100**, 11207 (1996).

Johansson, M. K.-J., Gray, S. M. and Johansson, L. S. O., "Studies of Low Coverage Adsorption of Li on Si(001): Observation of Negative Differential Resistance and Electron Trapping," *J. Vac. Sci. Technol. B*, **14**, 1015 (1996).

Kaba, M. S., Song, I. K. and Barteau, M. A., "Ordered Array Formation and Negative Differential Resistance Behavior of Cation-exchanged Heteropoly Acids Probed by Scanning Tunneling Microscopy," *J. Phys. Chem.*, **100**, 19577 (1996).

Kaba, M. S., Song, I. K. and Barteau, M. A., "Investigation of Framework and Cation Substitutions in Keggin-type Heteropoly Acids Probed by Scanning Tunneling Microscopy and Tunneling Spectroscopy," *J. Vac. Sci. Technol. A*, **15**, 1299 (1997).

Kaba, M. S., Song, I. K., Duncan, D. C., Hill, C. L. and Barteau, M. A., "Molecular Shapes, Orientation, and Packing of Polyoxometalate Arrays Imaged by Scanning Tunneling Microscopy," *Inorg. Chem.*, **37**, 398 (1998).

Kaba, M. S., Barteau, M. A., Lee, W. Y. and Song, I. K., "Nanoscale Characterization of Acid Properties of Heteropolyacids by Scanning Tunneling Microscopy and Tunneling Spectroscopy," *Appl. Catal. A*, **194**, 129 (2000).

Kaba, M. S., Song, I. K. and Barteau, M. A., "Site Identification of Mixed Arrays of Keggin-type Heteropolyacids (HPAs) by Scanning Tunneling Microscopy and Tunneling Spectroscopy," *J. Phys. Chem. B*, **106**, 2337 (2002).

Keggin, J. F., "Structure of the Molecule of 12-Phosphotungstic Acid," *Nature*, **131**, 908 (1933).

Kim, H. C., Moon, S. H. and Lee, W. Y., "Nature of the Effect of Counter Cations on the Redox Property of 12-Molybdophosphates," *Chem. Lett.*, 447 (1991).

Kinne, M. and Barteau, M. A., "STM and TS Investigations of Silver Polyoxometalate Monolayers: Model Compounds and Potential Multifunctional Oxidation Catalysts," *Surf. Sci.*, **447**, 105 (2000).

Kozhevnikov, I. V., "Heteropoly Acids and Related Compounds as Catalysts for Fine Chemical Synthesis," *Catal. Rev.-Sci. Eng.*, **37**, 311 (1995).

Lee, H. J. and Ho, W., "Structure Determination by Single-molecule Vibrational Spectroscopy and Microscopy: Contrast between Copper and Iron Carbonyls," *Phy. Rev. B*, **61**, R16347 (2000).

Lee, J. K., Song, I. K. and Lee, W. Y., "Separation of H_2/CO by the Selective Sorption Property of $H_3PMo_{12}O_{40}$ Embedded in PVA Membrane," *Korean J. Chem. Eng.*, **12**, 384 (1995).

Lee, W. Y., Song, I. K., Lee, J. K., Park, G. I. and Lim, S. S., "Design of Heteropoly Compound-imbedded Polymer Film Catalysts and Their Application," *Korean J. Chem. Eng.*, **14**, 432 (1997).

Lee, W. Y. and Song, I. K., "Design of Heteropolyacid-imbedded Polymer Films and Catalytic Membranes," *HWAHAK KONGHAK*, **38**, 317 (2000).

Maboudian, R., Carraro, C. and Weinberg, W. H., "Resonant Scanning Tunneling Spectroscopy of a Quantum-well Heterostructure," *Surf. Sci. Lett.*, **280**, L263 (1993).

Misono, M., "Heterogeneous Catalysis by Heteropoly Compounds of Molybdenum and Tungsten," *Catal. Rev.-Sci. Eng.*, **29**, 269 (1987).

Okuhara, T., Hu, C., Hashimoto, M. and Misono, M., "Acid Strength of Heteropolyacids and Its Correlation with Catalytic Activity," *Bull. Chem. Soc. Jpn.*, **67**, 1186 (1994).

Okuhara, T., Mizuno, N. and Misono, M., "Catalytic Chemistry of Heteropoly Compounds," *Adv. Catal.*, **41**, 113 (1996).

Park, G. I., Lee, W. Y. and Song, I. K., "MTBE Synthesis by Keggintype and Dawson-type Heteropolyacids," *HWAHAK KONGHAK*, **38**, 155 (2000).

Pope, M. T. and Müller, A. (Eds.), "Polyoxometalates: from Platonic Solids to Anti-retroviral Activity," Kluwer Academic Publishers, Dordrecht, The Netherlands (1994).

Sadakane, M. and Steckhan, E., "Electrochemical Properties of Polyoxometalates as Electrocatalysts," *Chem. Rev.*, **98**, 219 (1998).

Silva, S. L., Patel, A. A., Pham, T. M. and Leibsle, F. M., "Scanning Tunneling Microscopy Studies of Methoxy and Formate on Cu(110) Surfaces Resulting from Reactions with Methyl Formate, Methanol, and Formic Acid," *Surf. Sci.*, **441**, 351 (1999).

Song, I. K., Moon, S. H. and Lee, W. Y., "Catalytic Properties of Ther-

mally Decomposed 12-Molybdophosphoric and 10-Molybdo-2-vanadophosphoric Acids," *Korean J. Chem. Eng*., **8**, 33 (1991).

Song, I. K., Kaba, M. S. and Barteau, M. A., "STM Investigation of Pyridine Interaction with Heteropoly Acid Monolayers," *J. Phys. Chem*., **100**, 17528 (1996).

Song, I. K., Kaba, M. S., Barteau, M. A. and Lee, W. Y., "Scanning Tunneling Microscopy of Self-assembled Heteropoly Acid Monolayers Deposited on Graphite Surface: NDR Behavior and Redox Activity," *HWAHAK KONGHAK*, **35**, 407 (1997).

Song, I. K., Kaba, M. S., Barteau, M. A. and Lee, W. Y., "Investigation of Redox Potential and Negative Differential Resistance Behavior of Heteropolyacids by Scanning Tunneling Microscopy," *Catal. Today*, **44**, 285 (1998).

Song, I. K. and Barteau, M. A., "Bulk Redox Properties of Heteropolyacids (HPAs) Determined from Surface Properties of Nanostructured Heteropolyacid Monolayers," *J. Mol. Catal. A*, **182-183**, 185 (2002).

Song, I. K., Shnitser, R. B., Cowan, J. J., Hill, C. L. and Barteau, M. A., "Nanoscale Characterization of Redox and Acid Properties of Keggin-type Heteropolyacids by Scanning Tunneling Microscopy and Tunneling Spectroscopy: Effect of Heteroatom Substitution," *Inorg. Chem*., **41**, 1292 (2002).

Steltenpohl, A. and Memmel, N., "Adsorption Site of Oxygen on Pd (111)," *Surf. Sci*., **443**, 13 (1999).

Stipe, B. C., Rezaei, M. A., Ho, W., Gao, S., Persson, M. and Lundqvist, B. I., "Single-Molecule Dissociation by Tunneling Electrons," *Phy. Rev. Lett*., **78**, 4410 (1997).

Stipe, B. C., Rezaei, M. A. and Ho, W., "Single-molecule Vibrational Spectroscopy and Microscopy," *Science,* **280**, 1732 (1998).

Strandberg, R., "Multicomponent Polyanions. 13. The Crystal Structure of a Hydrated Dodecamolybdophosphoric Acid, $H_3Mo_{12}PO_{40}$ $(H_2O)_{29-31}$," *Acta Chem. Scand. A*, **29**, 359 (1975).

Tanaka, K. and Ozami, A., "Acid-Base Properties and Catalytic Activity of Solid Surfaces," *J. Catal*., **8**, 1 (1967).

Watson, B. A., Barteau, M. A., Haggerty, L., Lenhoff, A. M. and Weber, R. S., "Scanning Tunneling Microscopy and Tunneling Spectroscopy of Ordered Hetero- and Iso-polyacid Arrays on Graphite," *Langmuir*, **8**, 1145 (1992).

Weber, R. S., "Molecular Orbital Study of C-H Bond Breaking during the Oxidative Dehydrogenation of Methanol Catalyzed by Metal Oxide Surfaces," *J. Phys. Chem*., **98**, 2999 (1994).

Wouda, P. T., Nieuwenhuys, B. E., Schmid, M. and Varge, P., "Chemically Resolved STM on a PtRh(100) Surface," *Surf. Sci*., **359**, 17 (1996).